UNIVERSITÄT AUGSBURG
Universitätsbibliothek

OPEN ACCESS
OPUS AUGSBURG

Deconfinement transition and dimensional crossover in the Bechgaard-Fabre salts: pressure- and temperature-dependent optical investigations

Alexej Pashkin, Martin Dressel, M. Hanfland, Christine A. Kuntscher

Angaben zur Veröffentlichung / Publication details:

Pashkin, Alexej, Martin Dressel, M. Hanfland, and Christine A. Kuntscher. 2010. "Deconfinement transition and dimensional crossover in the Bechgaard-Fabre salts: pressure- and temperature-dependent optical investigations." *Physical Review B* 81 (12): 125109. https://doi.org/10.1103/physrevb.81.125109.

Nutzungsbedingungen / Terms of use:

licgercopyright

Dieses Dokument wird unter folgenden Bedingungen zur Verfügung gestellt: / This document is made available under these conditions:
Deutsches Urheberrecht
Weitere Informationen finden Sie unter: / For more information see:
https://www.uni-augsburg.de/de/organisation/bibliothek/publizieren-zitieren-archivieren/publiz/

Deconfinement transition and dimensional crossover in the Bechgaard-Fabre salts: Pressure- and temperature-dependent optical investigations

A. Pashkin,[1,*] M. Dressel,[2] M. Hanfland,[3] and C. A. Kuntscher[1,†]
[1]*Experimentalphysik II, Universität Augsburg, Universitätsstr. 1, 86159 Augsburg, Germany*
[2]*1. Physikalisches Institut, Universität Stuttgart, Pfaffenwaldring 57, 70550 Stuttgart, Germany*
[3]*European Synchrotron Radiation Facility, BP 220, 38043 Grenoble, France*
(Received 25 September 2009; revised manuscript received 22 December 2009; published 8 March 2010)

The infrared response of the organic conductor $(TMTSF)_2PF_6$ and the Mott insulator $(TMTTF)_2PF_6$ are investigated as a function of temperature and pressure and for the electric field polarized parallel and perpendicular to the molecular stacks. By applying external pressure on $(TMTTF)_2PF_6$, the Mott gap rapidly diminishes until the deconfinement transition occurs when the gap energy is approximately twice the interchain transfer integral. In its deconfined state $(TMTTF)_2PF_6$ exhibits a crossover from a quasi-one-dimensional to a higher-dimensional metal upon reducing the temperature. For $(TMTSF)_2PF_6$ this dimensional crossover is observed either with increase in external pressure or with decrease in temperature. We quantitatively determine the dimensional crossover line in the pressure-temperature diagram based on the degree of coherence in the optical response perpendicular to the molecular stacks.

DOI: 10.1103/PhysRevB.81.125109 PACS number(s): 71.30.+h, 78.30.Jw, 62.50.−p, 61.05.cp

I. INTRODUCTION

The physics of one-dimensional (1D) conductors is substantially different compared to two- or three-dimensional systems. Theory shows that the effects of electronic interaction in an electron gas have to be treated in a completely different way in one dimension compared to three dimensions. The resulting non-Fermi-liquid metallic state is called the Luttinger-liquid (LL) state;[1–3] it is characterized by a vanishing step in the occupation function leading to a power-law behavior in numerous physical quantities. In the case of a half-filled conduction-band Coulomb repulsion results in a 1D Mott insulating state. These phenomena are realized in highly anisotropic systems consisting of well-separated chains or stacks of structural entities. In practice, however, a certain coupling between the 1D stacks is unavoidable, that can be described by a transverse hopping integral $t_\perp$. Since this implies a possible charge transport normal to the chains, the system becomes *quasi*-1D. If the interchain coupling is strong enough, i.e., if $t_\perp$ exceeds a critical value $t_\perp^*$, the Mott insulating state is suppressed.[3–7] In other words: for $t_\perp < t_\perp^*$ the single-particle interchain hopping is completely absent for $T=0$ and the system is a 1D Mott insulator (MI). In contrast, for $t_\perp > t_\perp^*$ interchain transport is present; the electrons are not confined to the stacks any more and the system is in a quasi-1D metallic state. The critical value $t_\perp^*$ for this deconfinement transition is given by the energy scale of the electronic correlations, i.e., $t_\perp^*$ should be comparable to the value of the Mott gap $\Delta_\rho \approx A t_\perp^*$ with the prefactor $A = 1.8-2.3$.[4]

Ideally, the deconfinement transition is a quantum phase transition that can take place at zero temperature when the interchain coupling is varied.[3] The Mott insulator becomes a correlated metal (two or three dimensional) due to the finite interchain coupling. The 1D LL state is the consequence of the smearing of the Fermi-Dirac distribution at high-enough temperatures to mask the warping of the open Fermi surface due to the interchain coupling $t_\perp$. Hence, the deconfinement at temperatures $T \gg t_\perp/k_B$ leads to a LL metallic state. When the interchain coupling becomes stronger, eventually a dimensional crossover from a LL to a higher-dimensional metallic state is induced; it can also be reached when the temperature drops. This dimensional crossover occurs when the warping of the Fermi surface (proportional to $t_\perp$) exceeds the energy of thermal fluctuations, i.e., $t_\perp > k_B T$. The higher-dimensional metallic state can be described by Fermi-liquid theory; its physical properties are distinctly different compared to the LL state.[8] All these phenomena are summarized in the phase diagram sketched in Fig. 1.

Well-known models of quasi-1D systems are the Fabre salts $(TMTTF)_2X$ and the Bechgaard salts $(TMTSF)_2X$.[9–11] They consist of molecular stacks formed by TMTTF or TMTSF cations (which stands for tetramethyltetrathiafulvalene and tetramethyltetraselenafulvalene, respectively).[12] Since half an electron is transferred from each organic mol-

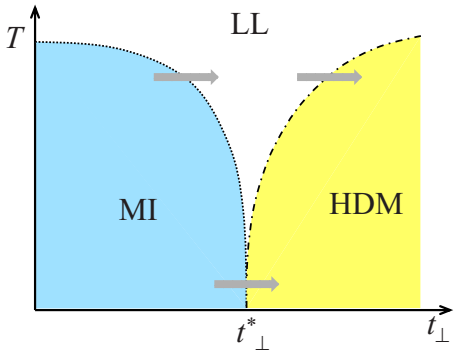

FIG. 1. (Color online) Schematic phase diagram of the deconfinement transition for a system of weakly coupled chains according to Refs. 3 and 7. The transition from a Mott insulator (MI) to a high-dimensional metallic (HDM) state occurs at $T=0$ when the transverse hopping integral $t_\perp$ reaches a critical value $t_\perp^*$. At high-enough temperature, the increase in $t_\perp$ leads to a transition from a Mott insulator to a 1D Luttinger-liquid (LL) state and, with further increase in $t_\perp$ to a dimensional crossover to a HDM.

 ©2010 The American Physical Society

ecule to the anions X^-, the band is three-quarter filled; the systems become effectively half filled because TMTSF and TMTTF form dimers. Charge transport occurs along the a axis due to overlap of electronic orbitals of sulfur or selenium atoms, respectively. The interstack separation is shortest in b direction and determined by two facts: (i) the size of the anions X^- and (ii) the extension of the chalcogen orbitals. The $(TMTTF)_2X$ salts have weaker interstack coupling and therefore are 1D Mott insulators. For the $(TMTSF)_2X$ salts, the interstack coupling is stronger resulting in a quasi-1D metallic state.

Applying external pressure to the crystals decreases the intermolecular distances; the consequences are twofold: (i) in stacking direction a the bands widen slightly and (ii) the interstack hopping integral t_b increases exponentially. Thus, it is expected that under pressure the electronic properties of $(TMTTF)_2X$ salts approach those of their TMTSF analogs. Over the years extensive experimental investigations of Bechgaard-Fabre salts made it possible to construct a generic temperature-pressure phase diagram[13,14] containing a variety of ground states (Mott insulator, spin Peierls, Luttinger liquid, superconducting, etc.). According to their ambient-pressure properties, all Bechgaard-Fabre salts with centrosymmetric anions (such as AsF_6, PF_6, or Br) can be located at certain position in the phase diagram. The pressure offset between $(TMTTF)_2PF_6$ and $(TMTSF)_2PF_6$, for instance, is about 3 GPa.[13] Thus, applying external pressure to the Mott insulator $(TMTTF)_2PF_6$ should induce a metallic state similar to the one in $(TMTSF)_2PF_6$.

The first experimental evidence that relates the Mott gap Δ_ρ to the transverse hopping term $t_\perp^*$ at the deconfinement transition was accomplished by comparing the Mott gap (obtained by ambient-pressure infrared spectroscopy) for various Bechgaard-Fabre salts with anions of different size to the interstack hopping integrals estimated from tight-binding calculations.[15] Vescoli *et al.* suggested that the deconfinement transition takes place around the region where $2t_b \approx \Delta_\rho$. Obviously, due to the limited number of compounds only a few points on the pressure axis can be simulated by chemical pressure. Moreover, the substitution of anions affects not only the interstack coupling but also the dimerization, and thus the band structure, along the stacks. A direct proof of the predicted deconfinement transition and a quantitative determination of the dimensional crossover is highly desired.

External pressure is known to be a clean way to tune the relevant parameters of a system. Hence, infrared spectroscopy under external pressure is the superior method to explore the deconfinement transition experimentally: here, the changes in the electrodynamic response along different directions can be monitored while the interstack coupling is continuously raised. We recently applied this method to obtain a first glance on the deconfinement transition in the Bechgaard-Fabre salts.[16,17] Since this study was restricted to room temperature and the frequency range was limited, the size of the Mott gap as a function of pressure could only be inferred rather than directly obtained.

The one dimensionality of the Bechgaard-Fabre salts has a crucial impact on their electronic properties in the deconfined state which is described by the LL model. The dimensional crossover between quasi-1D and high-dimensional (Fermi-liquid) electronic states shown in Fig. 1 is very interesting regarding theoretical[7,18,19] and experimental[20–23] aspects. Several power law exponents characterizing the energy and temperature dependence of the conductivity change at the dimensional crossover.[19,22] The best pronounced signature is expected for the transverse resistivity in the direction of the weakest interchain coupling (c axis in case of the Bechgaard-Fabre salts). This transverse charge transport can be described in terms of incoherent tunneling between the conducting chains. Since the density of states available for the tunneling obey qualitatively different behavior in case of Luttinger and Fermi liquids the transverse resistivity is expected to show a maximum at the dimensional crossover, which indeed has been observed in several experiments.[20–22] High-pressure measurements allowed Moser *et al.*[20] to trace the dimensional crossover temperature T^* as a function of pressure P for $(TMTSF)_2PF_6$. The observed $T^*(P)$ dependence is rather strong and nonlinear pointing to a renormalization due to correlation effects. The verification of the $T^*(P)$ dependence by an alternative method would be an important step in the characterization of the electronic correlation effects in quasi-1D systems. As already pointed out by Jacobsen *et al.*[24] optical data provide a convenient possibility to determine the dimensionality of the electronic system and thus to identify the dimensional crossover. Thus, probing the interchain infrared response under external pressure offers a promising alternative to the dc transport measurements.

In this paper we present the results of an extensive temperature-dependent infrared study of the organic salts $(TMTTF)_2PF_6$ and $(TMTSF)_2PF_6$ under external pressure. These data combined with the pressure-dependent unit-cell constants determined by x-ray diffraction (XRD) measurements allowed us to directly obtain the values of the Mott gap Δ_ρ and the interstack hopping integral t_b as a function of pressure. Thus we were able to verify the relation between Δ_ρ and t_b at the point of the deconfinement transition in $(TMTTF)_2PF_6$. Furthermore, we estimate the line of the dimensional crossover in the temperature-pressure diagram of $(TMTTF)_2PF_6$ and $(TMTSF)_2PF_6$. Based on the obtained results, we quantitatively suggest a unified phase diagram for the studied Bechgaard-Fabre salts.

The paper is organized as follows. Section II gives a brief description of the experimental techniques. The x-ray diffraction data are shortly presented in Sec. III A. Section III B contains the infrared spectroscopy results. The pressure-dependent values of the Mott gap and the transverse hopping integral are given in Sec. IV A and discussed in terms of the pressure-induced deconfinement transition. Section IV B discusses the infrared response along the b' direction in terms of the interstack transport coherence. The dependence of the so-called coherence parameter on pressure and temperature is presented and the lines of the dimensional crossover are determined. Finally, Sec. V summarizes the results within a unified temperature-pressure phase diagram.

II. EXPERIMENT

Single crystals of $(TMTTF)_2PF_6$ and $(TMTSF)_2PF_6$ were grown by a standard electrochemical growth procedure. The

measured samples had as-grown specular surfaces in *ab* plane and a thickness of about 50 μm. The room-temperature polarized infrared reflectivity was measured in the range 200–8000 cm^{-1} using a Bruker IRscope II microscope attached to a Bruker IFS66v/S Fourier-transform spectrometer. The measurements in the far-infrared range (200–700 cm^{-1}) were performed at the infrared beamline of the synchrotron radiation source ANKA. A diamond-anvil cell (DAC) (Ref. 25) equipped with type IIA diamonds suitable for infrared measurements was used to generate pressures up to 6 GPa. Finely ground CsI powder was chosen as quasihydrostatic pressure-transmitting medium.

The midinfrared (mid-IR) reflectivity (580–8000 cm^{-1}) at low temperature and high pressure was measured using a home-built infrared microscope coupled to the spectrometer and maintained at the same vacuum conditions in order to avoid absorption lines of H_2O and CO_2 molecules. The infrared radiation was focused on the sample by all-reflecting homemade Schwarzschild objectives with a large working distance of about 55 mm and 14× magnification. The DAC was mounted on the cold finger of a continuous flow helium cryostat (CryoVac KONTI) with two metallic rods, which allow mechanical access to the DAC lever arm mechanism. Thus, the pressure in the DAC could be changed *in situ* at arbitrary temperature.

In all high-pressure measurements the pressure in the DAC was determined *in situ* by the ruby luminescence method.[26] More details about the geometry of the reflectivity measurements and the Kramers-Kronig analysis of the data can be found in our earlier publications.[16,27]

In addition we carried out room-temperature XRD experiments at beamline ID09A of the European Synchrotron Radiation Facility at Grenoble. Liquid helium served as pressure-transmitting medium. The DAC rotation angle varied from −30° to +30° for $(TMTTF)_2PF_6$ and from −20° to +20° for $(TMTSF)_2PF_6$ with 2° step. The diffraction patterns of the single crystals have been analyzed using the XDS package.[28] The details are given in Ref. 29.

III. RESULTS

A. X-ray diffraction

The single-crystal XRD data show that the space-group symmetry $P\bar{1}$ of both studied compounds[30,31] remains intact up to pressures of 6–8 GPa.[29] The dependence of unit-cell volume of $(TMTTF)_2PF_6$ and $(TMTSF)_2PF_6$ is shown in Fig. 2. The change of the unit-cell volume can be fitted with the Birch equation of state,[32]

$$P(V) = \frac{3}{2}B_0(x^7 - x^5)\left[1 + \frac{3}{4}(B_0' - 4)(x^2 - 1)\right] \qquad (1)$$

with $x=(V/V_0)^{1/3}$ and V_0 denotes the unit-cell volume at ambient pressure. The values of the bulk modulus B_0 obtained from the fits are 7.27 ± 0.64 GPa and 12.71 ± 0.97 GPa for $(TMTTF)_2PF_6$ and $(TMTSF)_2PF_6$, respectively. The corresponding pressure derivatives of the bulk modulus B_0' are 9.98 ± 1.15 and 4.23 ± 0.75, respectively. Our findings agree with previous structural studies of $(TMTSF)_2PF_6$ under moderate pressure.[31,33]

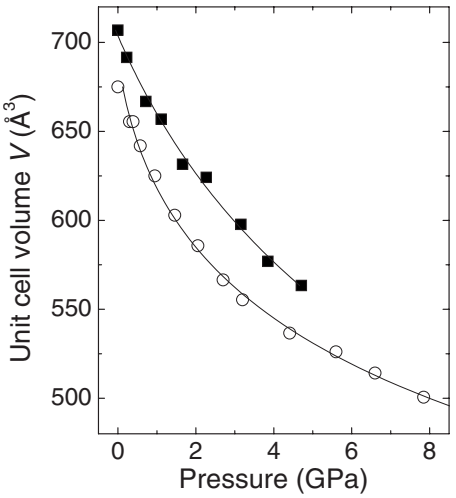

FIG. 2. Pressure-dependent unit-cell volume of $(TMTTF)_2PF_6$ (open circles) and $(TMTSF)_2PF_6$ (full rectangles) at room temperature. The lines represent the fits according to the Birch equation of state, Eq. (1).

The Bechgaard-Fabre salts exhibit a strong thermal expansion[31] that has to be taken into account, for instance, when dc transport experiments are compared with theoretical predictions of some power-law behavior on $\rho(T)$.[22,34] We acknowledge this dependence also in our present analysis of the optical conductivity (see Sec. III B). The underlying idea is that the reduction in the unit-cell volume is achieved either by applying pressure or by reducing the temperature. Utilizing the temperature dependence of the unit-cell parameters of $(TMTSF)_2PF_6$ measured at ambient pressure[31] we obtain a relation between temperature and the pressure of 2.3×10^{-3} GPa/K, assuming linearity. This means, for example, that cooling down by 100 K at ambient pressure is equivalent to applying 0.23 GPa pressure. By assuming that this relation is also valid at high pressures and the sulfur analog, we were able to estimate the unit-cell volume at any point of the temperature-pressure phase diagram for the analysis of our infrared spectroscopic results.

B. Infrared optical response

1. Parallel to the stacks

Figure 3 displays the room-temperature reflectivity spectra measured at the sample-diamond interface, $R_{s\text{-}d}$, for radiation polarized along the stack ($\mathbf{E} \| a$). The data extend down to 200 cm^{-1} by combining spectra measured with a standard globar source with those using the synchrotron radiation. At around 2000 cm^{-1} the reflectivity is strongly influenced by multiple phonon absorption in the diamond anvil that causes artifacts in the spectra. Therefore, this frequency region is cut out and interpolated for the analysis. For $(TMTTF)_2PF_6$ the reflectivity spectra [Fig. 3(a)] consist of a strong mid-IR band and a number of sharp vibrational modes below 2000 cm^{-1}, which correspond to electron-molecular-vibration (emv)-coupled totally symmetric vibrations of the TMTTF molecules and infrared-active modes of the PF_6 anion.[35] The strong pressure dependence of $R_{s\text{-}d}$ agrees with

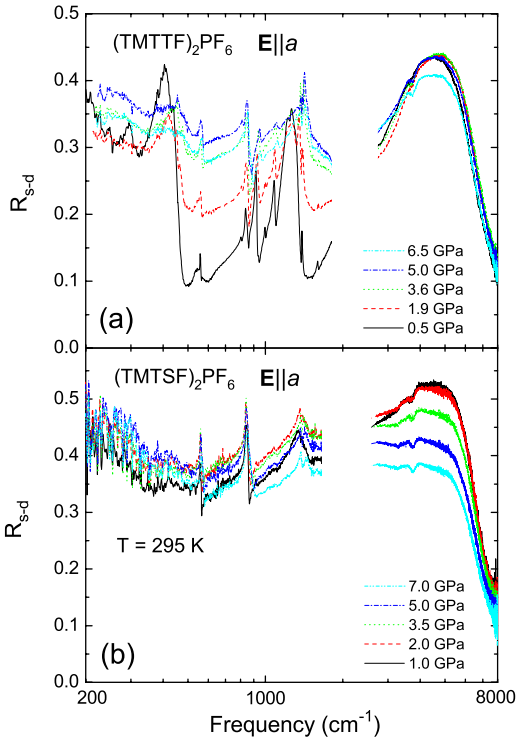

FIG. 3. (Color online) Pressure-dependent reflectivity spectra $R_{s\text{-}d}$ of $(TMTTF)_2PF_6$ and $(TMTSF)_2PF_6$ measured at room temperature for the polarization $\mathbf{E}\|a$.

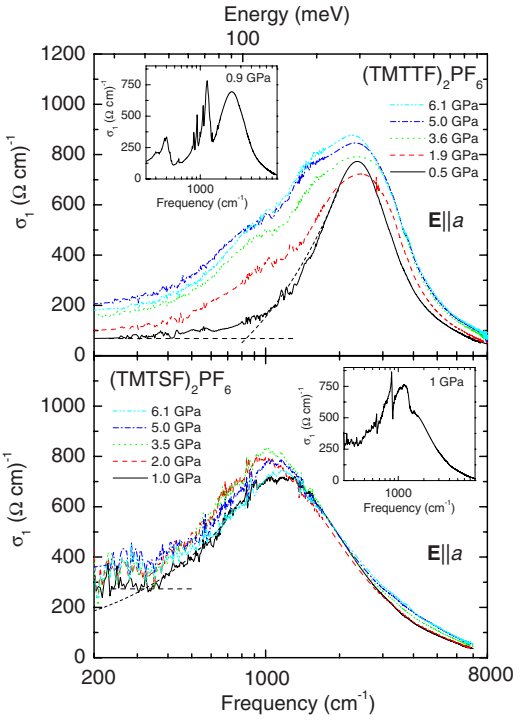

FIG. 4. (Color online) Real part of the optical conductivity σ_1 of $(TMTTF)_2PF_6$ and $(TMTSF)_2PF_6$ obtained from the room-temperature reflectivity for the polarization $\mathbf{E}\|a$. For clarity reason the phonon contributions are subtracted; examples of the complete conductivity spectra of $(TMTTF)_2PF_6$ and $(TMTSF)_2PF_6$ at low pressure are plotted in the insets. The dashed lines illustrate the method used to determine the Mott gap.

our previous findings on the sister compound $(TMTTF)_2AsF_6$.[16,17] Most important, the low-frequency reflectivity (below 1700 cm^{-1}) increases with pressure when the Mott gap vanishes; at the same time the vibrational modes shift to higher frequencies and broaden considerably.

In the case of $(TMTSF)_2PF_6$, the reflectivity spectra show similar features as observed for $(TMTTF)_2PF_6$ at pressures above 3 GPa [Fig. 3(b) compared to Fig. 3(a)]. Interestingly, the emv modes are less pronounced compared to TMTTF because the dimerization of the stacks in $(TMTSF)_2PF_6$ is much weaker.[35,36] The pressure-induced changes in the $(TMTSF)_2PF_6$ reflectivity are rather small and mainly consist in a decrease in the mid-IR feature.

The corresponding room-temperature conductivity spectra are obtained from the $\mathbf{E}\|a$ reflectivity by means of Kramers-Kronig analysis. The real part of the optical conductivity σ_1 of $(TMTTF)_2PF_6$ and $(TMTSF)_2PF_6$ at low pressure is shown in the insets of Fig. 4. For both materials the most pronounced feature is an absorption band in the mid-IR due to excitations of charge carriers from the lower to the upper Hubbard band. In order to disentangle the electronic and vibrational contributions to the optical conductivity, we fit the spectra with the Drude-Lorentz model, taking into account the Fano line shapes[37] of the emv-coupled modes. Then, the phonon contributions are subtracted and the resulting conductivity spectra are plotted in Fig. 4 for selected pressures.[38] With increasing pressure the $\mathbf{E}\|a$ optical conductivity of $(TMTTF)_2PF_6$ undergoes considerable changes with a large increase in spectral weight in the frequency range <8000 cm^{-1} due to the enlarged bandwidth. The enhancement is linear with pressure but saturates above 5 GPa (not shown). In addition, the spectral weight, as determined by the center of gravity of $\sigma_1(\omega)$ in the region plotted in Fig. 4(a), shifts to lower energies. Accordingly, the value of the Mott gap decreases. The size of the Mott gap Δ_ρ is estimated by the intersection between the linear extrapolation of the low-frequency edge of the Mott-Hubbard band and the constant background level of low-frequency conductivity, as illustrated by the dashed lines in Fig. 4. In contrast, the optical conductivity of $(TMTSF)_2PF_6$ exhibits only minor changes with pressure; the Mott-Hubbard band and the free-carrier motion along the molecular stacks are almost pressure independent. The pressure dependence of the Mott gap Δ_ρ for $(TMTTF)_2PF_6$ and $(TMTSF)_2PF_6$ is depicted in Fig. 10 and will be discussed in detail in Sec. IV A.

2. Perpendicular to the stacks

In Fig. 5 we show the reflectivity spectra of $(TMTTF)_2PF_6$ and $(TMTSF)_2PF_6$ measured for $\mathbf{E}\|b'$ at selected pressures. In general the absolute value is significantly lower compared to the corresponding data along the stacks and $R_{s\text{-}d}$ barely exceeds 0.25 in the measured spectral range. At the lowest applied pressure the reflectivity spectrum of $(TMTTF)_2PF_6$ is almost flat in the midinfrared range with an increase in the far infrared [Fig. 5(a)]. The response does not change with pressure up to 2 GPa. In this range, $(TMTTF)_2PF_6$ remains in the confined state and the coherent

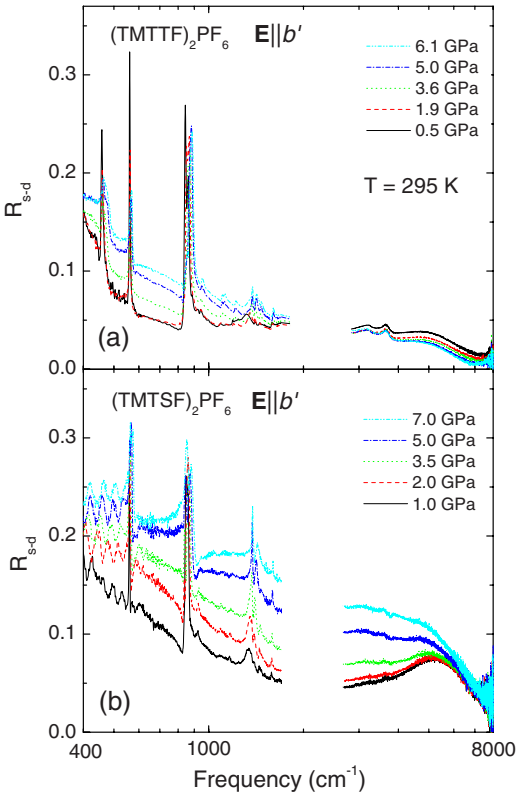

FIG. 5. (Color online) Pressure-dependent reflectivity spectra $R_{s\text{-}d}$ of $(TMTTF)_2PF_6$ and $(TMTSF)_2PF_6$ measured at room temperature for the polarization $\mathbf{E}\|b'$.

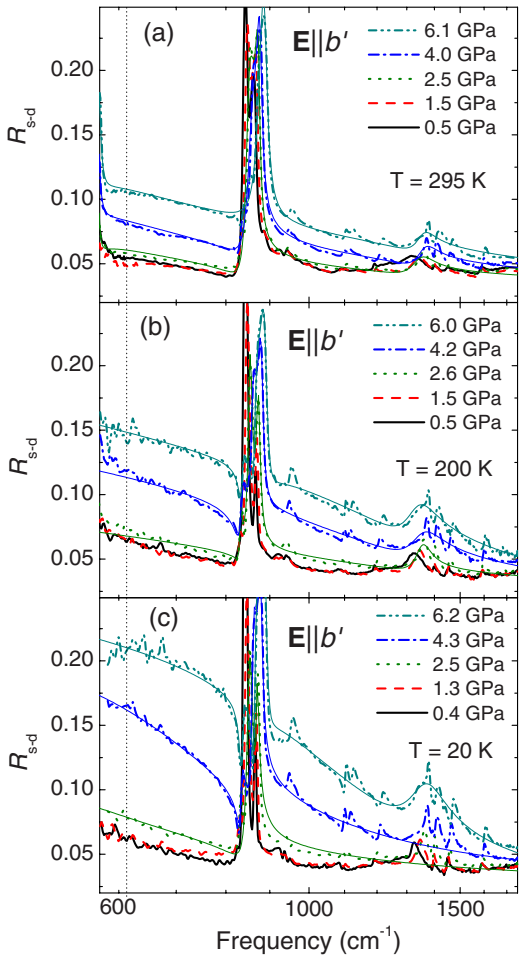

FIG. 6. (Color online) Pressure-dependent reflectivity spectra $R_{s\text{-}d}$ of $(TMTTF)_2PF_6$ for the electric field polarized normal to the stacks, $\mathbf{E}\|b'$, (a) at room temperature, (b) at 200 K, and (c) at 20 K. The vertical dotted line marks the frequency of 610 cm^{-1} at which the reflectivity change $\delta R_{s\text{-}d}$ is estimated (see Fig. 7). The solid lines are fits with a Drude term combined with Fano oscillators.

interstack transport is suppressed.[39] Only above 2 GPa the overall reflectivity increases and the spectrum develops a shape typical for a conductor; i.e., the reflectivity increases towards lower frequencies. This indicates the deconfinement of the interstack charge transport: above the critical pressure a coherent Drude response sets in for $\mathbf{E}\|b'$. $(TMTSF)_2PF_6$ [Fig. 5(b)] is in the deconfined state already at ambient pressure; thus the reflectivity continuously increases as pressure is applied. In contrast to the $(TMTTF)_2PF_6$ salt, no threshold at a critical pressure is observed in case of $(TMTSF)_2PF_6$.

The Drude response in the deconfined state of $(TMTTF)_2PF_6$ (i.e., above 2 GPa) changes its character with temperature. As seen in Fig. 6(a) for $T=295$ K the low-frequency reflectivity increases only slightly with decreasing frequency, which is typical for an overdamped Drude response when the relaxation rate exceeds the plasma frequency. In contrast, the Drude behavior gets more pronounced in the low-temperature reflectivity spectra [Figs. 6(b) and 6(c)]; the low-frequency reflectivity strongly increases with decreasing frequency and a well-defined plasma edge develops.

Figure 7 displays the normalized changes in the reflectivity values $R_{s\text{-}d}$ observed at 610 cm^{-1} as a function of pressure for three different temperatures. The reflectivity change is defined as $\delta R_{s\text{-}d}=(R_{s\text{-}d}-R^l_{s\text{-}d})/(R^h_{s\text{-}d}-R^l_{s\text{-}d})$, where $R^l_{s\text{-}d}$ and $R^h_{s\text{-}d}$ are the sample-diamond reflectivity at the lowest and highest applied pressures. Clearly, $\delta R_{s\text{-}d}$ starts to increase only above a certain threshold: the deconfinement transition in $(TMTTF)_2PF_6$ can unambiguously be identified at about 2 GPa. The coherent response leading to this Drude behavior increases as the temperature is reduced, the critical pressure of the deconfinement transition remains basically temperature independent.

For the Bechgaard salt $(TMTSF)_2PF_6$ the interstack transport changes continuously with pressure or temperature as seen from reflectivity spectra in Fig. 8. The Drude-type optical response at the lowest applied pressure becomes more pronounced on cooling down indicating the onset of coherent electronic transport between the stacks. This observation agrees with earlier ambient-pressure infrared studies[24,40,41] and it is discussed quantitatively in Sec. IV B. At pressures above 2 GPa and for temperatures below 100 K a plasma edge is clearly observed in the midinfrared range [Figs. 8(b) and 8(c)].

For a quantitative analysis of the transverse response, we fit the reflectivity spectra of $(TMTTF)_2PF_6$ and $(TMTSF)_2PF_6$ with the Drude model

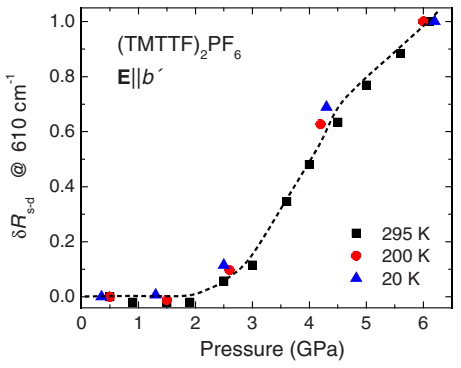

FIG. 7. (Color online) Normalized pressure-induced change in the reflectivity level of $(TMTTF)_2PF_6$ for $\mathbf{E}\|b'$ at 610 cm^{-1} at different temperatures as indicated. The dashed line is a guide to the eye.

$$\sigma(\omega) = \frac{\epsilon_0 \omega_p^2}{\Gamma - i\omega} \tag{2}$$

for the coherent transport and several Fano oscillators[37] describing intramolecular vibration modes. In Eq. (2) the plasma frequency is denoted by ω_p and the scattering rate by Γ. The fitting curves for the corresponding experimental $\mathbf{E}\|b'$ reflectivity spectra are displayed in Figs. 6 and 8. From the fits, we obtained the real part of the optical conductivity for both salts, which is presented in Fig. 9 for several selected pressures. The room-temperature spectra of $(TMTTF)_2PF_6$ are fitted only in the deconfined phase (i.e., above 2 GPa) since the Drude response is supposed to be absent when the electrons are confined to the stacks. It is clear from Fig. 9 that for both salts the interstack conductivity strongly increases with pressure.

We also consider the pressure-dependent spectral weight, calculated according to

$$SW = \int_0^{\omega_c} \sigma_1(\omega) d\omega \tag{3}$$

for $\mathbf{E}\|b'$ as a function of pressure, where the cutoff is chosen as $\omega_c = 8000$ cm^{-1}. As expected, the spectral weight of $(TMTTF)_2PF_6$ is significantly smaller compared to $(TMTSF)_2PF_6$, however, it shows a stronger pressure dependence (see insets of Fig. 9). Already at ambient pressure the electrons are not confined in the stacks of $(TMTSF)_2PF_6$; consequently, the spectral weight is relatively high for $\mathbf{E}\|b'$. Furthermore, its pressure dependence is weaker and it saturates at high pressures. The values of the spectral weight allows us to estimate the transverse hopping integral t_b, as discussed in Sec. IV A. Furthermore, the parameters of the Drude response for $\mathbf{E}\|b'$ show the signatures of the expected temperature- and pressure-induced dimensional crossover, which will be considered in Sec. IV B.

IV. DISCUSSION

A. Deconfinement transition

The interstack infrared reflectivity spectra displayed in Fig. 6 provide clear indications of the pressure-induced deconfinement transition in $(TMTTF)_2PF_6$ at 2 GPa, as summarized in Fig. 7. We now compare our experimental findings with the theoretical predictions for the deconfinement transition, in particular, the relation between the Mott gap energy Δ_ρ and the interstack transfer integral t_b.

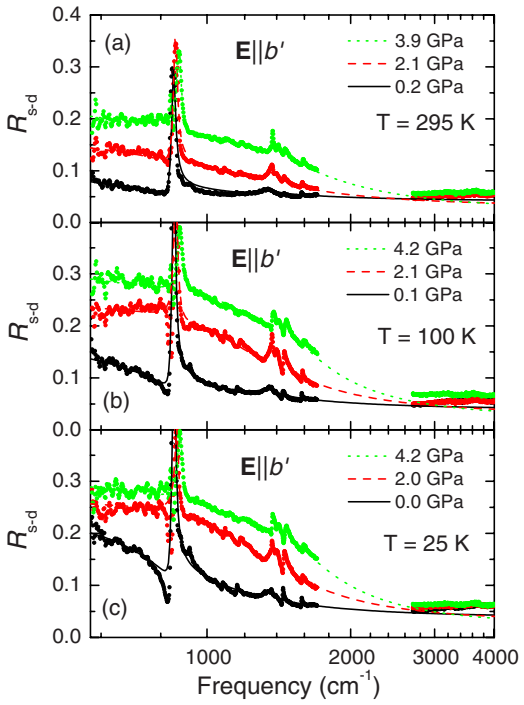

FIG. 8. (Color online) Pressure-dependent reflectivity spectra $R_{s\text{-}d}$ of $(TMTSF)_2PF_6$ for $\mathbf{E}\|b'$ (a) at room temperature, (b) at 100 K, and (c) at 25 K. The solid lines are fits with a Drude term combined with Fano oscillators.

First let us consider the in-stack optical response: the evolution of Δ_ρ as a function of pressure, determined from the $\mathbf{E}\|a$ conductivity spectra as described in Sec. III B 1, is displayed in Fig. 10 for both salts under investigation. The dramatic decrease in Δ_ρ in $(TMTTF)_2PF_6$ on approaching the deconfinement transition at 2 GPa is in excellent agreement with theoretical studies[42] and supported by earlier experiments.[21] It is interesting to note that the gap does not vanish completely above the transition; this was already inferred by earlier investigations on $(TMTSF)_2PF_6$.[43] The theory of the Mott transition in quasi-1D systems predicts that the gap may persist in the metallic phase.[44,45] By comparing both compounds under investigation, the values of the Mott gap for $(TMTSF)_2PF_6$ match well with the data for $(TMTTF)_2PF_6$, if we take into account a pressure offset of 3.0 GPa between the two salts; this value is in accordance with the generic temperature-pressure phase diagram of the Bechgaard-Fabre salts.[13]

Next we discuss the optical response perpendicular to the stacks: the pressure-dependent values of the interstack transfer integral t_b are obtained by the quantitative analysis of the transverse optical response. To this end we calculate the values of t_b using the plasma frequencies ω_p obtained from the Drude fits. At ambient conditions, both salts are quasi-1D compounds with an open Fermi surface, and the transverse hopping integral t_b is given by[46]

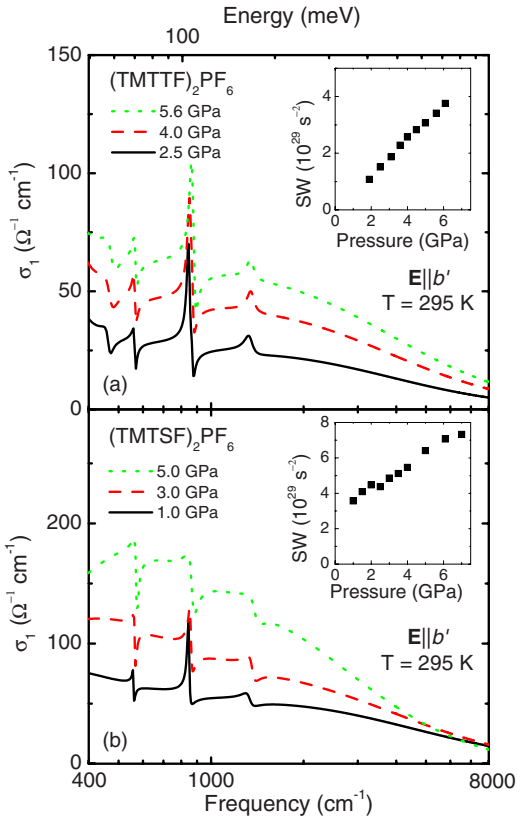

FIG. 9. (Color online) Real part of the optical conductivity σ_1 of (a) $(TMTTF)_2PF_6$ and (b) $(TMTSF)_2PF_6$ obtained from the fits of room-temperature reflectivity for the polarization $\mathbf{E}\|b'$. Insets show the respective spectral weight as a function of pressure obtained according to Eq. (3) when integrating up to 8000 cm^{-1}.

$$t_b^2 = \frac{\pi\epsilon_0\hbar^2 V_c t_a \omega_p^2}{4e^2 b^2}, \tag{4}$$

where V_c denotes the unit-cell volume, b the separation of the stacks, and t_a the transfer integral along the stacks. The geometrical parameters V_c (Fig. 2) and b were obtained by pressure-dependent x-ray diffraction measurements.[29] The value of t_a was calculated from the spectral weight of the in-stack optical conductivity using a simple tight-binding model.[16]

The calculated transverse hopping integral t_b is depicted in Fig. 10 as a function of pressure. The values of t_b for $(TMTTF)_2PF_6$ and $(TMTSF)_2PF_6$ perfectly agree with each other, taking into account a pressure offset of 3 GPa between these compounds.[47] Above the deconfinement transition (i.e., $P>2$ GPa) and up to 4 GPa the increase in t_b for $(TMTTF)_2PF_6$ is almost linear with a slope of 5 meV/GPa, in accord with our earlier results for $(TMTTF)_2AsF_6$.[16,17] Above 4 GPa the pressure-induced increase in t_b becomes weaker ($\sim$2 meV/GPa) for $(TMTTF)_2PF_6$ and comparable to the low-pressure behavior of $(TMTSF)_2PF_6$.

Finally, the quantitative criterion $\Delta_\rho \approx 2t_b^*$ for the deconfinement transition[4] can be verified by comparing the pressure dependence of the charge gap Δ_ρ with that of $2t_b$ (see Fig. 10). The onset of the coherent electronic transport normal to the stacks occurs at around 2 GPa, where $\Delta_\rho \approx 2t_b$. This agrees very well with our conclusions drawn from the pressure-dependent reflectivity results shown in Fig. 6. Thus, the results of our pressure-dependent infrared spectroscopic study exhibit an overall consistency and support the theoretical picture[3,4,7] for the deconfinement transition in quasi-1D compounds.

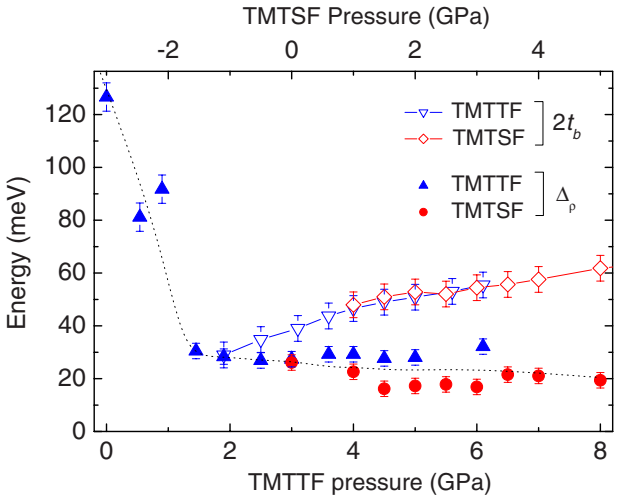

FIG. 10. (Color online) Pressure dependence of the Mott gap energy Δ_ρ and the transverse hopping integral $2t_b$ for $(TMTTF)_2PF_6$ and $(TMTSF)_2PF_6$ salts as obtained from the room-temperature data. The upper pressure scale corresponds to $(TMTSF)_2PF_6$ and is shifted by 3 GPa with respect to the lower pressure scale for the $(TMTTF)_2PF_6$ salt.

It is interesting to compare our results for the deconfinement transition induced by *external* pressure with the earlier findings obtained for anion substitution, i.e., the *chemical* pressure effect:[15] based on ambient-pressure infrared measurements, the Mott gap was deduced for several Bechgaard-Fabre salts and compared to the values of the interstack hopping integrals estimated from tight-binding calculations. The results strongly support our conclusion and the theoretical predictions that $2t_b \approx \Delta_\rho$ at the deconfinement transition.

B. Dimensional crossover

According to Sec. III B 2, for both compounds in the deconfined state one observed an enhancement of the Drude-type response along the b' direction when pressure is applied. Concomitant with the compression of the crystal lattice the orbital overlap between neighboring molecular stacks increases and hence the Drude response along the b' direction becomes stronger. On the other hand, upon lowering the temperature the scattering rate decreases, with a concomitant narrowing of the Drude term. Thus, at high pressure and low temperature the interstack transport is expected to be coherent and the dimensionality of the system should be enhanced (see Fig. 1). This dimensional crossover has drawn considerable interest in the theory of correlated electron systems of reduced dimensions.[48]

The trend towards a higher dimensionality with increasing pressure is illustrated by a comparison of the room-

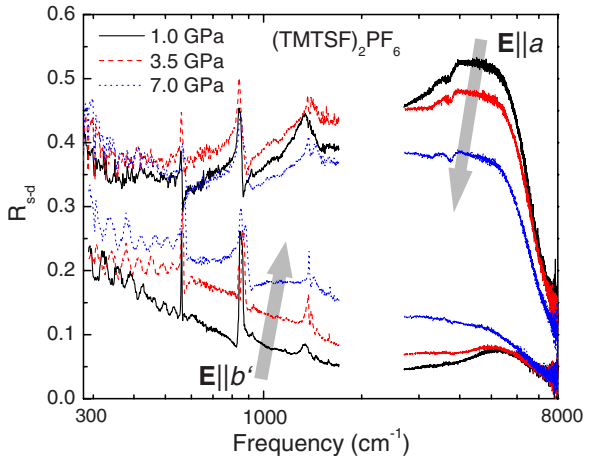

FIG. 11. (Color online) Comparison of the room-temperature reflectivity spectra $R_{s\text{-}d}$ of $(TMTSF)_2PF_6$ along and perpendicular to the stacks as pressure increases. The arrows indicate the major changes in the spectra with increasing pressure.

temperature infrared reflectivity spectra of $(TMTSF)_2PF_6$ for the polarization along and perpendicular to the stacking direction (see Fig. 11). Obviously, the anisotropy decreases with pressure: the Drude response starts to dominate the reflectivity for both polarizations and simultaneously the Mott-Hubbard band becomes less pronounced at high pressures. At the highest pressure (7 GPa) the reflectivity spectra along and perpendicular to the stacks are rather similar regarding the principle shape, especially their low-frequency part (below 1000 cm^{-1}). Thus, $(TMTSF)_2PF_6$ can readily be considered as a two-dimensional system at pressures around 7 GPa.

For a quantitative analysis of the dimensional crossover we now consider the degree of coherence of the charge transport. The hallmark of coherence is a Drude response with a plasma frequency exceeding the damping constant.[49] One can define a coherence parameter of the Drude response

$$\kappa = \frac{\omega_p}{2\Gamma}, \tag{5}$$

where ω_p and Γ are the plasma frequency and the scattering rate of the Drude term defined in Eq. (2). Coherent transport corresponds to $\kappa > \kappa^*$, while incoherent transport occurs for $\kappa < \kappa^*$, where κ^* is a critical value of the dimensional crossover which should be close to unity. The factor 2 in Eq. (5) stems from the analogy between the loss function of the Drude response and the response of a simple harmonic oscillator which is considered overdamped when its eigenfrequency is smaller than twice the damping constant.[50]

The above approach can be illustrated by the loss function

$$-\mathrm{Im}\left\{\frac{1}{\epsilon(\omega)}\right\} = \frac{\omega_p^2 \omega \Gamma}{(\omega^2 - \omega_p^2)^2 + \omega^2 \Gamma^2} \tag{6}$$

presented in Fig. 12 for various temperatures and pressures. In case of a Drude response the loss function has a Lorentzian line shape where the peak position corresponds to the plasma frequency ω_p and the width of the peak corresponds to the electron scattering rate Γ.[51] Thus, the sharpness of this

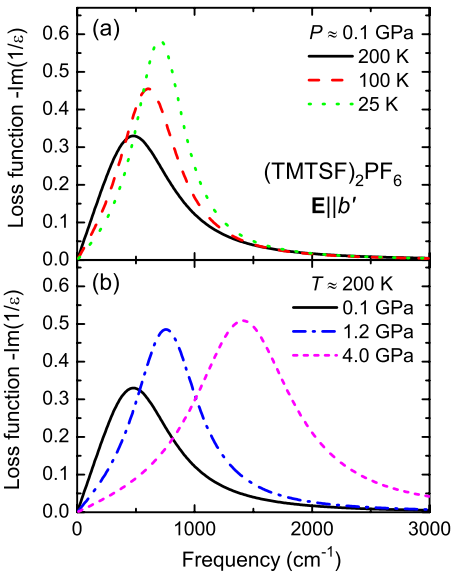

FIG. 12. (Color online) Loss function of the Drude response perpendicular to the conducting stacks ($\mathbf{E} \| b'$) in $(TMTSF)_2PF_6$: (a) at 0.1 GPa and three selected temperatures; (b) at 200 K and three selected pressures.

so-called plasmon peak in the loss function characterizes the degree of coherence of the charge transport. Figure 12(a) demonstrates the evolution of the plasmon peak for $\mathbf{E} \| b'$ in $(TMTSF)_2PF_6$ at the lowest applied pressure at selected temperatures. For 200 K the peak is clearly overdamped. Upon cooling its width decreases, resulting in a well-developed plasmon at 25 K. The plasmon peak exhibits a small blueshift with temperature decrease. Its evolution with pressure is significantly different: for a fixed temperature the plasmon peak strongly shifts to higher frequencies while the peak width only slightly increases [see Fig. 12(b)]. Thus, also the pressure application results in an underdamped plasmon peak. In conclusion, there are two ways to tune the dimensionality of the system and hence induce a dimensional crossover to a high-dimensional metallic (HDM) state, either by decreasing the temperature or by increasing the pressure.

The evolution of the dimensionality of $(TMTSF)_2PF_6$ is summarized in Fig. 13, where we plot the coherence parameter κ_b for $(TMTSF)_2PF_6$ as a function of temperature and pressure, determined from the Drude fits of the interstack reflectivity spectra. The large number of experimental data points in the diagram (six temperatures for each of the six pressure values) provides a rather detailed information on how the coherent transport develops. The highest degree of coherence is achieved for high pressures and low temperatures (lower right corner of the diagram). It gradually decreases as the pressure is released and the temperature is simultaneously raised towards the upper left corner of the diagram. The lines of constant coherence level are almost linear with pressure for $\kappa_b > 1$, however, for $\kappa_b < 1$ they become sublinear. In order to define the critical κ^* values that characterize the dimensional crossover, we utilize the experimental results of Moser *et al.*,[20] where the dimensional crossover temperature in $(TMTSF)_2PF_6$ at ambient pressure is proposed to be located at $T^* \approx 100$ K, in accordance with

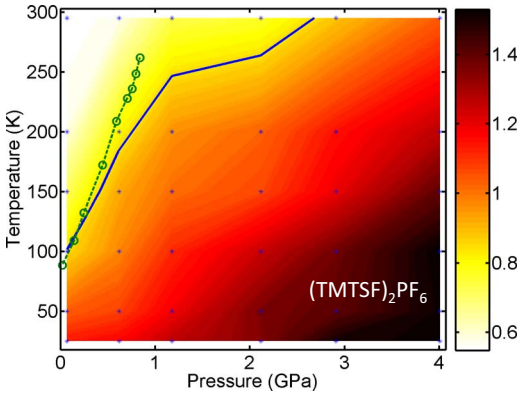

FIG. 13. (Color online) The coherence parameter of the interstack charge transport κ_b as a function of temperature and pressure for $(TMTSF)_2PF_6$. The solid line corresponds to $\kappa_b=0.85$. The circles illustrate the line of the dimensional crossover determined from transport measurements by Moser *et al.* (Ref. 20). The dotted line is a guide to the eye. The asterisks mark the measurement points.

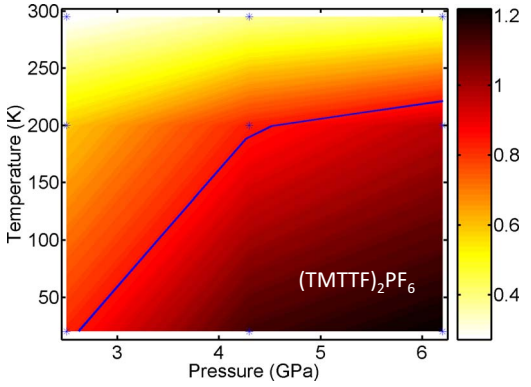

FIG. 14. (Color online) The coherence parameter of the interstack charge transport κ_b as a function of temperature and pressure for $(TMTTF)_2PF_6$. The solid line corresponds to $\kappa_b=0.85$. The asterisks mark the measurement points.

other dc and microwave measurements of the c^*-axis resistivity.[22,52] Using this as a reference point, we obtain the critical coherence parameter $\kappa_b \simeq 0.85$ based on our $(TMTSF)_2PF_6$ data measured at the lowest pressure ($\sim$0.2 GPa). The constant level line $\kappa_b \simeq 0.85$, i.e., the "crossover line," is depicted in Fig. 13. For pressures below 1.2 GPa the crossover line exhibits a remarkable strong slope, not expected in the naive picture of noninteracting electrons where $T^* \propto t_b$. According to Fig. 10 the interstack transfer integral t_b in $(TMTSF)_2PF_6$ increases only by about 30% when pressure increases by 4 GPa. Thus, one would expect the crossover temperature of about 130 K at 4 GPa for noninteracting electrons, in contrast to the experimental observation. This provides evidence that electronic correlations play a decisive role in the renormalization of the dimensional crossover in the Bechgaard salts, leading to the very fast suppression of the 1D state in favor of a high-dimensional metallic state. Unfortunately, the complete theoretical description of this phenomenon is still not elaborated.[19]

The strong increase in the crossover temperature with pressure is in agreement with the results of Moser *et al.*[20] deduced from dc transport. The results of these earlier investigations are included in Fig. 13 for comparison. In contrast to the almost linear crossover line based on the dc transport results, our infrared spectroscopic measurements yield a sublinear behavior with a tendency of saturation towards higher pressures (see Fig. 13). This sublinear behavior could be a consequence of the nonlinear pressure dependence of t_b which shows the tendency for saturation (see Fig. 10 and discussion in Sec. IV A) together with renormalization effects due to electronic interactions. However, we cannot completely rule out a certain effect of the nonperfect hydrostaticity in our measurements due to the solid pressure-transmitting medium, especially at high pressures; this may contribute to the observed increase in the scattering rate of the Drude response, which lowers the coherence parameter and shifts the dimensional crossover line down to lower temperatures.

A corresponding temperature-pressure diagram of the coherence parameter κ_b is depicted in Fig. 14 for $(TMTTF)_2PF_6$ in the deconfined state, i.e., for $P>2$ GPa. Due to the limited pressure range, the number of experimental points amounts to three temperatures for each of the three pressure values. According to Fig. 14 the coherence parameter demonstrates a temperature and pressure dependence similar to that of the $(TMTSF)_2PF_6$ salt. In Fig. 14 we include the dimensional crossover line following the critical value deduced for the $(TMTSF)_2PF_6$ salt $\kappa_b=0.85$. Also in the case of $(TMTTF)_2PF_6$ this crossover line exhibits a sublinear character and agrees rather well with the crossover line of the selenium analogue shifted by 3 GPa along the pressure

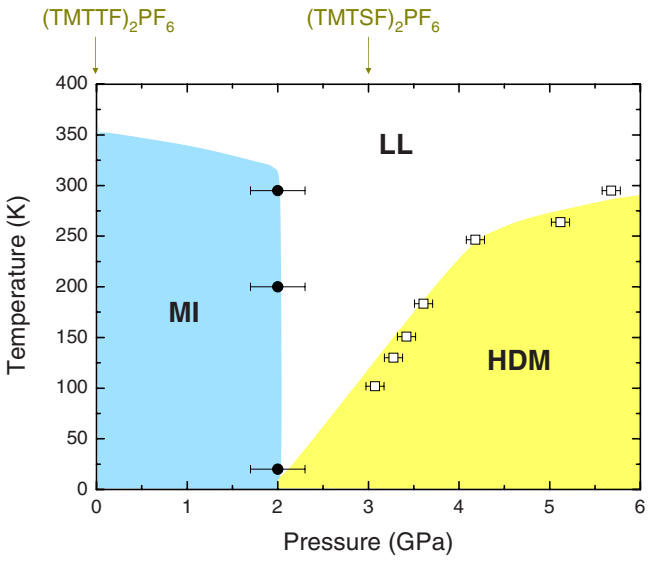

FIG. 15. (Color online) Temperature-pressure phase diagram of the Bechgaard-Fabre salts under investigation. The symbols represent the phase boundaries determined in this work: the deconfinement transition (solid circles) from the MI into the 1D LL, and the dimensional crossover (open squares) from the LL to the HDM state. For $(TMTTF)_2PF_6$ and $(TMTSF)_2PF_6$ the ambient-pressure positions are indicated.

scale. Thus, the chemical pressure offset of 3 GPa between the two studied salts in the generic phase diagram also holds for the occurrence of the dimensional crossover.

V. SUMMARY

Our comprehensive investigations of the infrared response of quasi-1D Bechgaard-Fabre salts as a function of pressure and temperature demonstrate that the pressure-induced deconfinement transition in the Mott insulator $(TMTTF)_2PF_6$ occurs at approximately 2 GPa. This critical pressure is basically temperature independent and it is characterized by the rapid onset of the interstack electronic transport (along the b' direction). The size of the Mott gap, Δ_ρ, rapidly decreases as the transition point is approached and stabilizes at a finite value upon further pressure increase. The deconfinement occurs when $\Delta_\rho \approx 2t_b$. These findings are in accordance with theoretical predictions and earlier experiments which utilized the effect of chemical pressure.

Furthermore, the dimensional crossover in the studied salts occurs when the coherence parameter of the interstack transport κ_b exceeds a critical value of 0.85. The crossover temperature increases rapidly with pressure, which evidences the importance of electronic correlations for the dimensional crossover. The line of the dimensional crossover is sublinear in the temperature-pressure diagram and saturates at high pressures.

Remarkably, the pressure offset between the dimensional crossover lines for $(TMTTF)_2PF_6$ and $(TMTSF)_2PF_6$ amounts to 3 GPa, i.e., the same as the corresponding offset between the values of the transverse hopping integral t_b. All the results obtained within this work can thus be included in a unified temperature-pressure phase diagram, which is presented in Fig. 15. The experimental points include the (P,T) values of the deconfinement transition in $(TMTTF)_2PF_6$ and the dimensional crossover line in $(TMTSF)_2PF_6$ shifted by 3 GPa along the pressure axis. Based on all data we schematically depict colored regions corresponding to different phases, namely, the Mott insulating, Luttinger liquid, and the high-dimensional metallic state.

ACKNOWLEDGMENTS

We thank G. Untereiner for crystal growth. We acknowledge the ESRF and ANKA facilities for the provision of beamtime and we would like to thank B. Gasharova, Y.-L. Mathis, D. Moss, and M. Süpfle for help at the IR beamline. We also would like to thank N. Drichko, M. Dumm, S. Ebbinghaus, T. Giamarchi, E. Rose, and K. Thirunavukkuarasu for fruitful discussions and K. Syassen for providing valuable information about the construction of the homemade infrared microscope. Financial support by the DFG (Emmy Noether-program, SFB 484, Grant No. DR228/27) is gratefully acknowledged.

*Present address: Fachbereich Physik, Unversität Konstanz, Universitätsstr. 10, 78457 Konstanz, Germany.
†christine.kuntscher@physik.uni-augsburg.de

[1] H. J. Schulz, Int. J. Mod. Phys. B **5**, 57 (1991).
[2] J. Voit, Rep. Prog. Phys. **58**, 977 (1994).
[3] T. Giamarchi, Chem. Rev. **104**, 5037 (2004).
[4] Y. Suzumura, M. Tsuchiizu, and G. Grüner, Phys. Rev. B **57**, R15040 (1998).
[5] M. Tsuchiizu, Y. Suzumura, and T. Giamarchi, Prog. Theor. Phys. **101**, 763 (1999).
[6] M. Tsuchiizu and Y. Suzumura, Phys. Rev. B **59**, 12326 (1999).
[7] S. Biermann, A. Georges, A. Lichtenstein, and T. Giamarchi, Phys. Rev. Lett. **87**, 276405 (2001).
[8] T. Giamarchi, *Quantum Physics in One Dimension* (Oxford University Press, Oxford, U.K., 2004).
[9] D. Jérome and H. J. Schulz, Adv. Phys. **31**, 299 (1982).
[10] T. Ishiguro, K. Yamaji, and G. Saito, *Organic Superconductors* (Springer, Berlin, 1998).
[11] D. Jérome, Chem. Rev. **104**, 5565 (2004).
[12] The crystals have triclinic symmetry. The a axis is along the stacks formed by the planar organic molecules, b' denotes the projection of the b axis perpendicular to a, and c^* is normal to the ab plane.
[13] C. Bourbonnais and D. Jérome, Science **281**, 1155 (1998).
[14] H. Wilhelm, D. Jaccard, R. Duprat, C. Bourbonnais, D. Jérome, J. Moser, C. Carcel, and J. M. Fabre, Eur. Phys. J. B **21**, 175 (2001).
[15] V. Vescoli, L. Degiorgi, W. Henderson, G. Grüner, K. P. Starkey, and L. K. Montgomery, Science **281**, 1181 (1998).
[16] A. Pashkin, M. Dressel, and C. A. Kuntscher, Phys. Rev. B **74**, 165118 (2006).
[17] A. Pashkin, C. A. Kuntscher, and M. Dressel, J. Low Temp. Phys. **142**, 563 (2006).
[18] A. Georges, T. Giamarchi, and N. Sandler, Phys. Rev. B **61**, 16393 (2000).
[19] T. Giamarchi, *The Physics of Organic Superconductors and Conductors* (Springer-Verlag, Berlin, 2008), Vol. 110, pp. 719–743.
[20] J. Moser, M. Gabay, P. Auban-Senzier, D. Jérome, K. Bechgaard, and J. M. Fabré, Eur. Phys. J. B **1**, 39 (1998).
[21] P. Auban-Senzier, D. Jérome, C. Carcel, and J. M. Fabre, J. Phys. IV **114**, 41 (2004).
[22] M. Dressel, K. Petukhov, B. Salameh, P. Zornoza, and T. Giamarchi, Phys. Rev. B **71**, 075104 (2005).
[23] P. Auban-Senzier, C. R. Pasquier, D. Jérome, S. Suh, S. E. Brown, C. Meziere, and P. Batail, Phys. Rev. Lett. **102**, 257001 (2009).
[24] C. S. Jacobsen, D. B. Tanner, and K. Bechgaard, Phys. Rev. Lett. **46**, 1142 (1981).
[25] R. Keller and W. B. Holzapfel, Rev. Sci. Instrum. **48**, 517 (1977); G. Huber, K. Syassen, and W. B. Holzapfel, Phys. Rev. B **15**, 5123 (1977).
[26] H. K. Mao, J. Xu, and P. M. Bell, J. Geophys. Res. **91**, 4673 (1986).
[27] C. A. Kuntscher, S. Frank, A. Pashkin, M. Hoinkis, M. Klemm, M. Sing, S. Horn, and R. Claessen, Phys. Rev. B **74**, 184402 (2006).

[28] W. Kabsch, J. Appl. Crystallogr. **26**, 795 (1993).
[29] A. Pashkin, M. Dressel, S. Ebbinghaus, M. Hanfland, and C. Kuntscher, Synth. Met. **159**, 2097 (2009).
[30] P. Delhaes, C. Coulon, J. Amiell, S. Flandrois, E. Torreilles, J. M. Fabre, and L. Giral, Mol. Cryst. Liq. Cryst. **50**, 43 (1979).
[31] B. Gallois, J. Gaultier, C. Hauw, and T.-D. Lamcharfi, Acta Crystallogr., Sect. B: Struct. Sci. **42**, 564 (1986).
[32] F. Birch, J. Geophys. Res. **83**, 1257 (1978).
[33] B. Gallois, J. Gaultier, T. Lamcharfi, F. Bechtel, A. Filhol, L. Ducasse, and M. Abderrabba, Synth. Met. **19**, 321 (1987).
[34] B. Korin-Hamzić, E. Tafra, M. Basletić, A. Hamzić, G. Untereiner, and M. Dressel, Phys. Rev. B **67**, 014513 (2003).
[35] C. S. Jacobsen, D. B. Tanner, and K. Bechgaard, Phys. Rev. B **28**, 7019 (1983).
[36] D. Pedron, R. Bozio, M. Meneghetti, and C. Pecile, Phys. Rev. B **49**, 10893 (1994).
[37] U. Fano, Phys. Rev. **124**, 1866 (1961).
[38] At high pressure the emv coupling becomes stronger and the phonons become more asymmetric and broader. Thus the fit of the phonon contributions is less perfect, leading to the weak shoulder around 800–1000 cm^{-1} in the spectra of $(TMTTF)_2PF_6$.
[39] dc experiments under pressure performed in the b' direction confirm this behavior: although the absolute value of the room-temperature resistivity decreases with pressure, $\rho(T)$ resembles an activating hopping transport at low pressure. E. Rose, M. Dumm, and M. Dressel (unpublished).
[40] L. Degiorgi, M. Dressel, A. Schwartz, B. Alavi, and G. Grüner, Phys. Rev. Lett. **76**, 3838 (1996).
[41] V. Vescoli, L. Degiorgi, M. Dressel, A. Schwartz, W. Henderson, B. Alavi, G. Grüner, J. Brinckmann, and A. Virosztek, Phys. Rev. B **60**, 8019 (1999).
[42] C. Berthod, T. Giamarchi, S. Biermann, and A. Georges, Phys. Rev. Lett. **97**, 136401 (2006).
[43] M. Dressel, A. Schwartz, G. Grüner, and L. Degiorgi, Phys. Rev. Lett. **77**, 398 (1996).
[44] T. Giamarchi, Physica B **230-232**, 975 (1997).
[45] A. Schwartz, M. Dressel, G. Grüner, V. Vescoli, L. Degiorgi, and T. Giamarchi, Phys. Rev. B **58**, 1261 (1998).
[46] J. F. Kwak, Phys. Rev. B **26**, 4789 (1982).
[47] Note that the spectral weights of the transverse-optical conductivity shown in the insets of Fig. 9 behave differently for both salts. Only the electronic hopping integrals calculated using pressure-dependent unit-cell parameters demonstrate agreement with the generic temperature-pressure phase diagram (Ref. 13).
[48] S. Biermann, A. Georges, T. Giamarchi, and A. Lichtenstein, *Proceedings of the NATO ASI: Field Theory of Strongly Correlated Fermions and Bosons in Low-Dimensional Systems*, (Windsor, 2001).
[49] This criterion was previously suggested by Jacobsen *et al.* (Ref. 24) to determine the temperature-induced dimensional crossover in $(TMTSF)_2PF_6$ at ambient pressure.
[50] G. Lucovsky, J. C. Mikkelsen, W. Y. Liang, R. M. White, and R. M. Martin, Phys. Rev. B **14**, 1663 (1976).
[51] M. Dressel and G. Grüner, *Electrodynamics of Solids* (Cambridge University Press, Cambridge, England, 2002).
[52] J. R. Cooper, L. Forro, B. Korin-Hamzic, K. Bechgaard, and A. Moradpour, Phys. Rev. B **33**, 6810 (1986).